IEEE Open Journal of
Industry Applications

Received 31 March 2024; revised 18 June 2024 and 2 July 2024; accepted 8 July 2024. Date of publication 17 July 2024; date of current version 5 August 2024. The review of this article was arranged by Associate Editor Giulia Tresca.

Digital Object Identifier 10.1109/OJIA.2024.3429518

Multiparallel Inverter Control Strategy for Grid-Supporting P2G Systems

GEDEON RUSATIRA [1,2], GAWOO PARK [2], AND KYUNGSOO LEE [1] (Member, IEEE)

[1]Energy and Electrical Engineering, Tech University of Korea, Siheung 15073, South Korea
[2]Research and Development Center, G-Philos.co., Ltd, Yongin 16983, South Korea

CORRESPONDING AUTHOR: KYUNGSOO LEE (email: kyungsoolee@tukorea.ac.kr).

This work was supported in part by the Research Project Fund of the Ministry of Oceans and Fisheries (MOF), in collaboration with the Korea Institute of Marine Science Technology Promotion (KIMST), under Grant 20220632 and in part by the 2021 sabbatical year research grant from the Tech University of Korea.

ABSTRACT This article introduces a novel control approach to obtain higher grid reliability using power-to-gas (P2G) conversion systems. The proposed control method named multiparallel vector current control is a variant of virtual synchronous machine (VSM) applied to the multiparallel inverter system (MPIS). It takes on the good qualities of VSM control, such as offering inertia, voltage support, the ability to operate in standalone mode, and strong performance in weaker grids. Moreover, this concept boasts swift current set-point tracking abilities and enhanced synchronization properties. Integration of the P2G system involves an MPIS that transforms ac power from renewable sources into usable dc power, along with an electrolysis device. The later utilizes dc power source to generate hydrogen and oxygen by decomposing water. This integration strategically prevents grid-induced overvoltage or undervoltage from affecting the electrolysis device. This protects it from malfunctions or damage while keeping the voltage and frequency within the normal range. The efficacy of the proposed control method is rigorously substantiated through analytical models, time-domain simulations, and experimental validation in real-world applications. This comprehensive validation process underscores its viability and robustness in ensuring grid stability while facilitating efficient P2G conversion operations.

INDEX TERMS Grid stability, multiparallel inverter, power-to-gas (P2G) systems, renewable energy integration, virtual synchronous machine.

NOMENCLATURE

Acronyms

P2G	Power-to-Gas.
VSM	Virtual synchronous machine.
MPIS	Multiparallel inverter system.
MP-VCC	Multiparallel vector current control.
RES	Renewable energy sources.
ZSCC	Zero-sequence circulating current.
GC / SA	Grid connected/Standalone.
VOC	Virtual oscillator control.
PLL	Phase-locked loop.
EMF	Electromotive force.
PCC	Point of common coupling.

Symbols

$P_E(t)/(P_E^*(t))$	Active power absorbed/reference by MPIS.
$P_R(t)$	Output power of renewable sources.
P_O	Operational threshold power of RES.
P_G	Grid's power demand.
$P_W(t)$	Active power command value.
$V_E(t)/I_E(t)$	Substation voltage/current.
$F_G(t)/V_G/I_G$	Frequency/voltage/current of the grid.
V_R/I_R	Output voltage/current of RES.
V_P	Voltage at general load connection point.
V_L/I_L	Voltage drop/current in transmission line.
R_L/X_L	Resistance/reactance of transmission line.

(ΔV_L)	Transmission line voltage drop.
$(\Delta V_L R)$	Transmission line voltage drop due to resistance.
$(\Delta V_L X)$	Transmission line voltage drop due to reactance.
v_e	Converter voltage.
ω_e/ω_g	Rotational frequency of converter voltage/PCC voltage.
v_g	Point of common coupling (PCC) voltage.
M	Virtual inertia.
k_D/k_G	Damper winding/Droop constants.
P_{set}	Power set-point.
ω_{set}	Angular frequency set-point.
P_e	Output power.
X	Converter filter reactance.
θ_e/θ_g	Phase angle of converter voltage/PCC voltage.
$k_{p\text{pll}}/k_{i\text{pll}}$	Proportional/integral gain of PLL.
$k_{p\text{sync}}/k_{i\text{sync}}$	Proportional/integral gain of synchronization control.
k_ω/k_v	Droop gain for frequency/voltage.
i_d^*/i_q^*	Real/imaginary-axis current reference.
κ	Proportionality constant.
G_M	Frequency droop control gain.
$G_{\text{avr}}(s)$	Transfer function of the automatic voltage restorer.
v_d/v_q	Real/imaginary-axis voltage.
v_s	Sensed voltage.
i_d/i_q	Real/imaginary-axis current.
$i_{d,\text{ff}}/i_{q,\text{ff}}$	Real/imaginary-axis current feedforward.
k_{comp}	Compensation gain.
α/β	Predetermined constants for power command.
n	Number of parallel inverters.

I. INTRODUCTION

A. MOTIVATION

The integration of renewable energy sources (RESs) into power systems represents a transformative shift towards sustainable energy production and has prompted the need for efficient energy storage solutions, among which power-to-gas (P2G) technology stands out [1], [2], [3], [4], [5]. However, this transition brings forth a host of challenges, notably impacting the stability of the grid. With RES penetration reaching unprecedented levels, concerns surrounding system inertia reduction and uncertainty in system capacity have escalated to the forefront of discussions among researchers and industry experts [6], [7]. P2G facilitates the conversion of surplus electricity from renewable sources into chemical energy carriers, such as hydrogen or synthetic natural gas. In P2G systems, inverters play a crucial role in converting electrical energy to a form suitable for electrolyzers or other conversion processes. However, the effective control of these inverters in distributed P2G systems poses significant challenges due to the dynamic nature of renewable energy generation and varying demand patterns. The increasing penetration of RESs has led to intermittent power generation, causing fluctuations in grid voltage and frequency. This variability necessitates advanced control strategies for inverters to maintain grid stability and ensure efficient energy conversion in P2G systems. In addition, the decentralized nature of P2G installations introduces complexities in coordinating multiple inverters to optimize system performance while mitigating potential grid disturbances. Consequently, there is a pressing need for novel control approaches tailored specifically to address the unique requirements of distributed P2G systems, ensuring seamless integration with RESs while maintaining grid stability under varying operating conditions.

B. LITERATURE REVIEW

Recent research endeavors have underscored the pivotal role of controlling inverter-interfaced energy resources in bolstering transient stability, particularly within microgrid contexts [8], [9], [10]. Various control strategies have emerged as promising approaches to support grid stability by effectively harmonizing voltage magnitude and frequency variation. Among these strategies, the main ones are droop control, VSM, and virtual oscillator control (VOC), each offering unique advantages and challenges.

Droop control presents a decentralized approach that enables distributed generation units to share load without the need for extensive communication protocols. However, its efficacy is hindered by limited virtual inertia, which can pose challenges in balancing power-sharing with voltage stability, particularly in standalone (SA) mode where grid support is absent [11], [12].

In contrast, VSM control represents a digital emulation of synchronous generator dynamics, boasting improved virtual inertia and self-synchronization capabilities without necessitating a phase-locked loop (PLL) [13], [14], [15], [16]. Despite its promise, there remains a notable gap in understanding how VSM strategies can be effectively applied to multiparallel inverter system (MPIS), which are increasingly relevant in modern grid architectures.

The VOC control concept introduces a nonlinear time domain controller that exhibits a faster primary control response, particularly advantageous in islanded microgrid scenarios. However, difficulties with secondary regulation and grid synchronization prevent the widespread adoption of VOC control, which restricts its practical application [17], [18], [19], [20], [21].

C. OBJECTIVE

The aim is to present a comprehensive solution that not only mitigates ZSCC and cross-circulating current issues but also enhances the overall performance and stability of MPIS for P2G integration. Although previous studies have focused on specific aspects of control or modulation techniques to address these challenges [22], [23], [24], this article takes a holistic approach by integrating advanced control algorithms with innovative hardware design considerations. By combining sophisticated control strategies with optimized hardware configurations, the proposed method seeks to achieve superior performance in terms of current sharing accuracy, dynamic response, and system reliability. Through rigorous analytical modeling, simulation studies, and experimental validation, this research aims to provide conclusive evidence of the effectiveness and practical feasibility of the proposed solution in real-world P2G applications. In addition, this article intends to offer insights into the underlying principles and mechanisms driving the proposed control scheme, thereby contributing to the broader understanding of inverter control strategies for renewable energy integration and grid stability enhancement.

D. CONTRIBUTIONS

Given the aforementioned challenges and opportunities, this article introduces a novel control approach designed to improve grid stability using P2G conversion systems. The following novelties are the main contributions of this research.

1) This article suggests a new way of controlling multi-parallel inverters, a variant of VSM control strategy, that offers a multifaceted solution. It inherits the beneficial characteristics of VSM control, such as providing inertia, voltage support, the ability to operate in SA mode, and robust performance in weaker grids. This is designed just for MPIS and can easily switch between grid-connected and SA operations.
2) Combining PLL and angle-synchronization loop to emulate the swing equation in the proposed MP-VCC scheme is a key part of this new approach. The goal is to make the inverter more stable and ensure that the ac-bus voltage stays stable in a range of operating conditions, with a focus on the use of P2G systems.
3) In addition, this concept features swift current setpoint tracking abilities and enhanced synchronization properties. A current compensation algorithm that prevents cross-circulating currents between parallel modules is included in MP-VCC, and its impact can be verified in SA operation.

Through these advances, the proposed control method aims to address critical challenges associated with grid stability and pave the way for widespread adoption of renewable energy integration in modern power systems and enabling green hydrogen production.

E. LIMITATIONS

The concept proposed in this research suggests a paradigm shift in MPIS operation. Traditionally, such devices relied on external power management systems to regulate key parameters, such as the voltage of the grid and the frequency. This regulation is typically achieved by absorbing active power through internal switching components, which are controlled by the external power management device.

However, the innovation introduced by this research lies in the MPIS's newfound ability to autonomously manage its operations. This means that it can regulate voltage and frequency without external intervention, thus reducing the dependence on external control systems.

The current implementation and validation are focused on specific MPIS configurations, necessitating further research to ensure scalability for larger and more diverse systems. In addition, although the control strategy performs well under tested conditions, its robustness under extreme dynamic load variations requires additional investigation.

The transition from traditional control systems to the proposed autonomous MPIS operation also poses integration challenges with existing grid infrastructure and power management systems. By addressing these limitations through future research, the proposed approach can be further optimized and applied to a broader range of renewable energy and P2G applications.

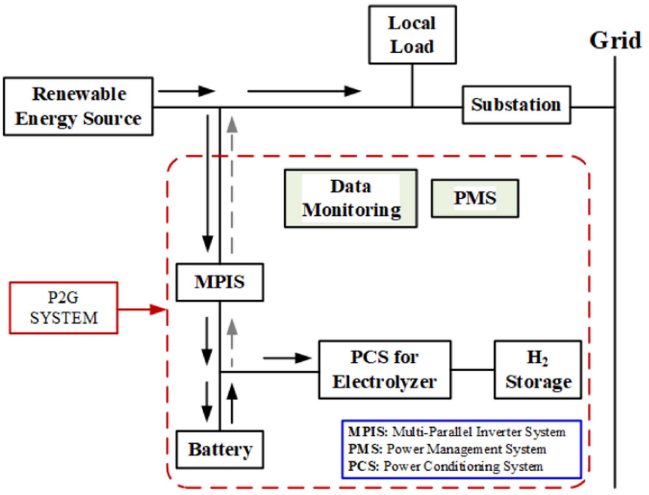

FIGURE 1. Structure of a typical P2G system.

By implementing this concept, the MPIS gains the agility to respond quickly to variations in grid frequency and voltage. This is a significant advancement, as it enables the device to dynamically adapt to changing grid conditions, ensuring stability and efficiency even in fluctuating environments.

In essence, this research presents a transformative approach to power conversion, where devices are empowered to control their operations, leading to improved performance, responsiveness, and overall grid stability.

The rest of this article is organized as follows. First, Section II describes the configuration and mathematical model of the presented system. Then, Section III discusses the control concept proposed in this article. The practical performance of the proposed control method is verified through experimental tests in Section IV. Finally, Section V concludes this article.

II. SYSTEM CONFIGURATION AND OPERATION REVIEW

Fig. 1 represents a schematic of a typical P2G system according to an embodiment of this research. The P2G system is installed between a RES and an adjacent substation. Hereafter, the substation is also referred to as the grid-connected system. The P2G system comprises an MPIS, an electrolyzer, and a power management device. In addition, the P2G system may include a hydrogen storage device and a monitoring device, which might also be situated externally to the P2G system, according to the embodiment. Normally, the MPIS converts ac power from the grid, received at the substation (also known as grid connection point A), into usable dc power for the electrolyzer. The electrolyzer receives power from the MPIS and utilizes it to electrolyze water, producing hydrogen and oxygen. Conventionally, the power management device controls the MPIS, the electrolyzer, and the monitoring

device. The monitoring device is linked to the power management device and measures substation voltage, substation current, and grid frequency, relaying this information to the power management device. It is important to note that the actual grid voltage and grid current measured in the grid at the grid connection point might differ from the substation voltage, substation current, and grid frequency measured by the monitoring device. Moreover, substation voltage and substation current serve as information for the power management device to detect changes in the grid measured at the grid connection point A. The power management device instructs the MPIS to supply the electrolyzer with excess active power that the grid cannot accommodate when the grid frequency rises. Similarly, when the grid frequency decreases, the power management device continuously reduces the operating active power of the MPIS to zero to avoid grid-related incidents. The power management device determines the command value for MPIS to absorb the active power from the RES based on the output power of the RES and the substation voltage. When exceeds the specified operational threshold power of the RES, this control helps to stabilize the substation voltage and the grid frequency by absorbing the excess active power of RES using the MPIS

$$P_w^*(t) = \alpha \times (P_R(t) - P0). \tag{1}$$

Furthermore, when the output power of the RES is below the operational threshold but exceeds the grid's power demand, the power management device can utilize a known value (β) to determine the minimum for MPIS using conventional control techniques

$$P_w^*(t) = v_e \times \beta \times (i_r(t) - i_g(t)). \tag{2}$$

Consequently, the MPIS operates according to the control of the power management device, stabilizing the grid's voltage and frequency by absorbing active power through the operation of internal switching components. The flowchart that mentions the step-wise implementation of the existing control commands is given in Fig. 2. However, with the proposed control concept in this research, the MPIS can manage its operations without depending on the power management device. This results in fast response to frequency and voltage variations.

Each inverter of MPIS, (cf., Fig. 3), consists of a filter section, a switching section, and a dc-link section. The filter section suppresses reflected waves transferred to the grid system by the switching operation. The switching section is a three-phase, three-level topology that converts ac to dc based on the substation voltage command, substation current command, and switching patterns instructed by the power management device controller, outputting the required voltage and current for the electrolyzer power conditioning unit. The dc-link section stabilizes the momentarily varying dc voltage during the switching operation. Moreover, the monitoring device may communicate with nearby RES to receive information regarding their output power, output voltage, and current and relay this data to the power management device as

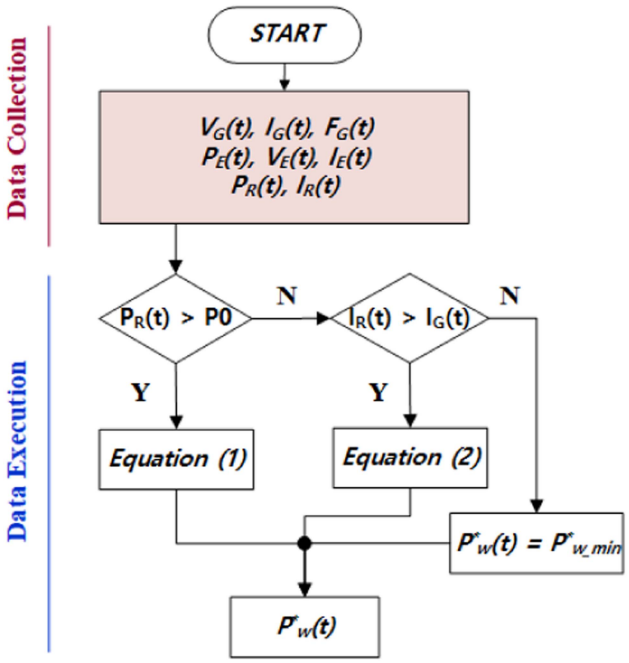

FIGURE 2. Flowchart of stepwise implementation of the existing P2G system.

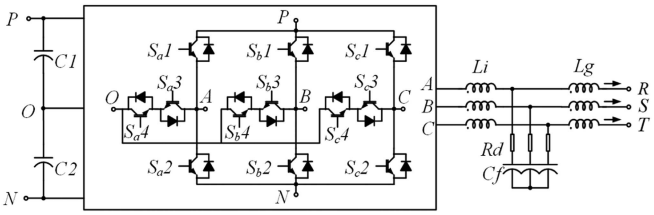

FIGURE 3. Module configuration in MPIS.

required. The battery guarantees stable P2G system operation and protects its internal components during grid disturbances. Its primary function is to safeguard against fluctuations in RES output connected to the MPIS, ensuring they do not impact system performance. In addition, it provides essential power for the electrolyzer, or MPIS, during grid faults. Controlled by the PMS, the battery can safely shut down the system if power becomes unavailable during operations, like a grid fault, while the MPIS is active.

Fig. 4(a) illustrates the connection point (A) of the P2G system is located between the RES and the ac grid system. Fig. 4(b) depicts the relationship between the output voltage of the RES, the substation voltage, and the voltage at the general load connection point (B).

The voltage fluctuation in the transmission line connected to the RES includes a voltage drop due to the resistance component of the transmission line and a voltage fluctuation due to the inductance of the transmission line [25], [26], because the transmission voltage is very high and the resistance value of the transmission line is low, the effective voltage drop

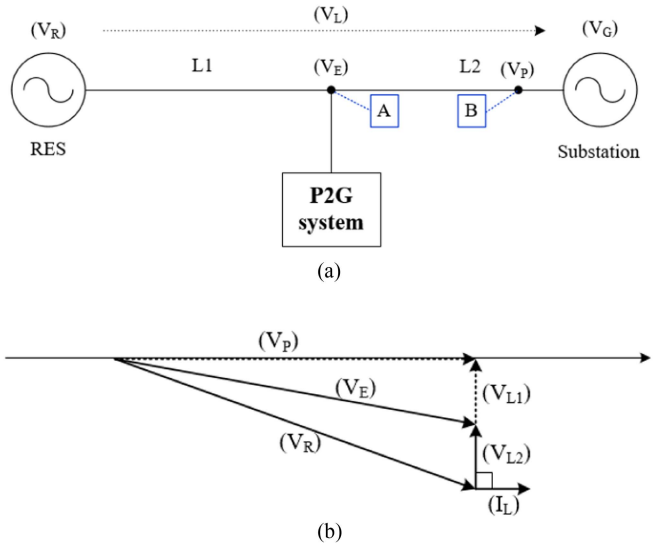

FIGURE 4. P2G system: (a) configuration between the RES and the ac grid and (b) relationship between voltages at each terminal.

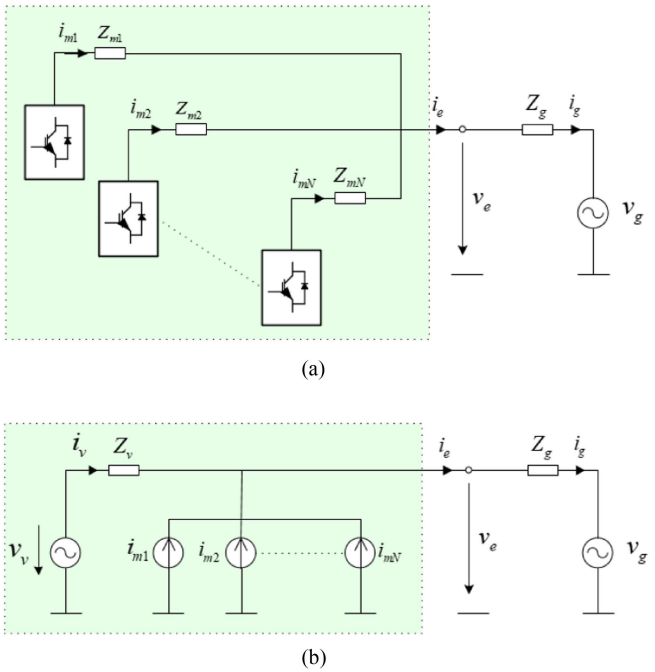

FIGURE 5. Equivalent models of (a) MPIS with grid-following control and (b) MPIS with grid-forming control.

due to the transmission line is very minimal. Hence, there exists a relationship between the output voltage of the RES and the voltage at the general load connection point (B), as represented by the equation as follows:

$$Z_L = -R_L + iX_L \tag{3}$$

$$\begin{aligned} V_L &= I_L \times Z_L \\ &= I_L \times (-R_L + iX_L) \\ &= -\Delta V_{LR} + i\Delta V_{LX} \end{aligned} \tag{4}$$

$$\begin{aligned} V_P &= V_R + V_L \\ &= V_R - \Delta V_{LR} + i\Delta V_{LX}. \end{aligned} \tag{5}$$

The voltage at the general load connection point (B) usually remains stable within a certain range due to the grid interconnection conditions. Normally, when the output power from the RES increases, the current flowing through the grid should also increase proportionally to the voltage at the general load connection point (B). However, as the grid current increases, the voltage drop across the transmission line also increases. This means that the output voltage from the RES injected into the grid to supply power would logically be higher than the voltage at the general load connection point.

Furthermore, the output power from the RES must have an equivalent phase to the output voltage at the grid interconnection point (A). In addition, the phase of the output voltage from the RES should reflect the voltage variation across the transmission line. As a result, the effective output of the RES becomes lower than the actual output. The above description can be represented mathematically, as shown in the following equations:

$$\begin{aligned} P_R &= V_R \times I_L \\ &= V_R \times I_R \times \cos\theta, (0 \le \cos\theta \le 1) \end{aligned} \tag{6}$$

$$P_W = V_W \times I_W. \tag{7}$$

The MPIS between the RES and the load connection point (B) should exhibit a voltage drop due to the transmission line (L1) that is lower than the total voltage drop at the load connection point (B). Consequently, the voltage supplied by the MPIS to the grid should be higher than that at the general load connection point

$$V_E \ge V_P. \tag{8}$$

As shown in the vector diagram in Fig. 4(b), the relationship described above can be extended to the expression (10)

$$V_L = V_{L1} + V_{L2} \tag{9}$$

$$\begin{aligned} V_E &= V_R + V_{L1} \\ &= V_R + (V_L - V_{L2}) \\ &= V_P + V_{L2}. \end{aligned} \tag{10}$$

III. CONTROL ARCHITECTURE DERIVATION

A. CONCEPT FORMULATION

Fig. 5(a) represents the equivalent models of MPIS with traditional control methods, and Fig. 5(b) is the equivalent circuit model after implementing the proposed control method. The proposed concept comprises two functional control elements on each module: an indirect voltage control for a virtual voltage source inverter operating in parallel with multiple virtual current sources inverters, as illustrated in Fig. 5(b). The master control, which does not have any appropriate switching

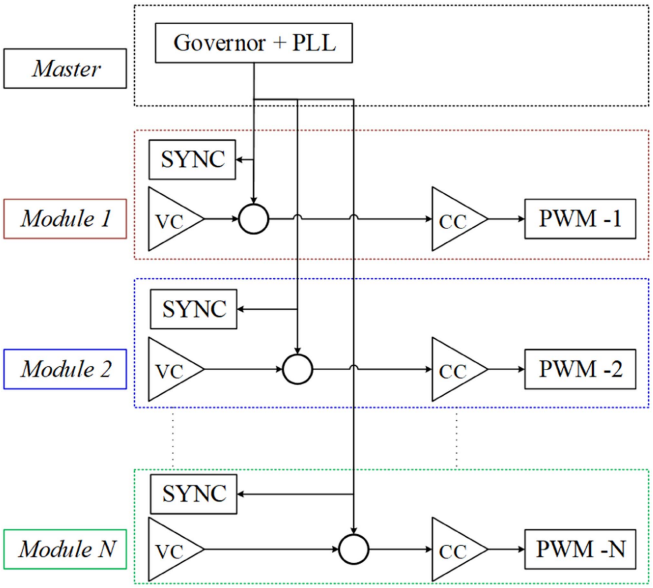

FIGURE 6. Control concept structure for MPIS.

module emulates the properties of the swing equation and governor using PLL, thus forming MP-VCC concept. The primary control mechanisms are the governor and automatic voltage restorer (AVR). They produce current references for the virtual current controllers of parallel inverter modules. The structural control concept of MPIS is given in Fig. 6.

The mechanical input power supplied to the proposed MP-VCC consistently originates from the power management device. Consequently, the system operates like virtual current sources in a stable condition. Moreover, it actively injects reactive power and aids in maintaining the bus voltage magnitude during steady-state operation. However, during transient intervals, the mechanical input power experiences brief fluctuations referred to as inertial power variations. The overall MP-VCC concept proposed for MPIS is given in Fig. 7.

B. SWING EQUATION

The swing equation links the frequency change of the back EMF to the machine's output power [27]. For a VSM without virtual stator impedance, the converter voltage matches the back EMF of the virtual machine. The converter filter impedance corresponds to the stator impedance of the virtual machine, and the PCC voltage matches the stator voltage of the virtual machine [28], [29]. The converter voltage rotates at a frequency that emphasizes its equivalence to the virtual rotor frequency. Similarly, the PCC voltage, or virtual stator voltage, also rotates at this frequency. The swing equation represents the dynamic behavior of synchronous generators in power systems and is given by

$$-M\frac{d\omega_r}{dt} = P_e + k_D(\omega_e - \omega_g) - P_{\text{set}} + k_G(\omega_e - \omega_{\text{set}}). \tag{11}$$

In the quasi-steady state, the output power is given by the angle difference between the virtual back EMF and the PCC voltage across the converter filter reactance

$$P_e = \frac{3}{2}\frac{v_e v_g}{X}\sin(\theta_e - \theta_g). \tag{12}$$

According to Narula et al. [27], the swing equation is formally equal to the PLL combined with the governor term. Equivalency between the PLL and the swing equation of a virtual synchronous generator is a concept used in power systems to model the behavior of inverters in current research

$$\sin(\theta_e - \theta_g) \approx (\theta_e - \theta_g) \tag{13}$$

$$s \cdot \sin(\theta_e - \theta_g) \approx (\omega_e - \omega_g). \tag{14}$$

Equation (11) can be rewritten as

$$\frac{d\omega_e}{dt} = -\frac{1}{M}\frac{3}{2}\frac{v_e v_g}{X}(\theta_e - \theta_g) - \frac{1}{M}k_D s(\theta_e - \theta_g) + \frac{1}{M}P_{set} - \frac{1}{M}k_G(\omega_e - \omega_{\text{set}}). \tag{15}$$

The PLL and angle synchronization are control systems used in power converters to synchronize their output voltage with the grid voltage. The mathematical representations of their dynamics are (15) and (17), respectively

$$\omega_e = \left(k_{p\text{pll}} + \frac{k_{i\text{pll}}}{s}\right) v_{g,q}(\theta_e - \theta_g) = \left(k_{p\text{pll}} + \frac{k_{i\text{pll}}}{s}\right) v_g \sin\theta_g \tag{16}$$

$$\theta_g = \int \omega_g dt \tag{17}$$

$$\omega_e = \left(k_{p\text{sync}} + \frac{k_{i\text{sync}}}{s}\right)(\theta_e - \theta_g) \tag{18}$$

$$\theta_e = \int \omega_e dt. \tag{19}$$

The dynamics of angle synchronization are the same as the swing equation's dynamics. This equivalence helps the power converter behave like a synchronous generator and contributes to grid stability. The relationship between the rotor angle and the PLL phase angle in a virtual synchronous generator can be established using control techniques, which may involve PLL algorithms or synchronization methods [30]. The exact mapping between the swing equation and PLL may vary based on the control strategy and specific system characteristics

$$\frac{d\omega_e}{dt} = (s \cdot k_{p\text{sync}} + k_{i\text{sync}})(\theta_e - \theta_g) = s \cdot k_{p\text{sync}}(\theta_e - \theta_g) + k_{i\text{sync}}(\theta_e - \theta_g) \tag{20}$$

$$k_{p\text{sync}} = -\frac{1}{M} \cdot k_D \tag{21}$$

$$k_{i\text{sync}} = -\frac{1}{M} \cdot \frac{3}{2} \cdot \frac{v_e v_g}{X}. \tag{22}$$

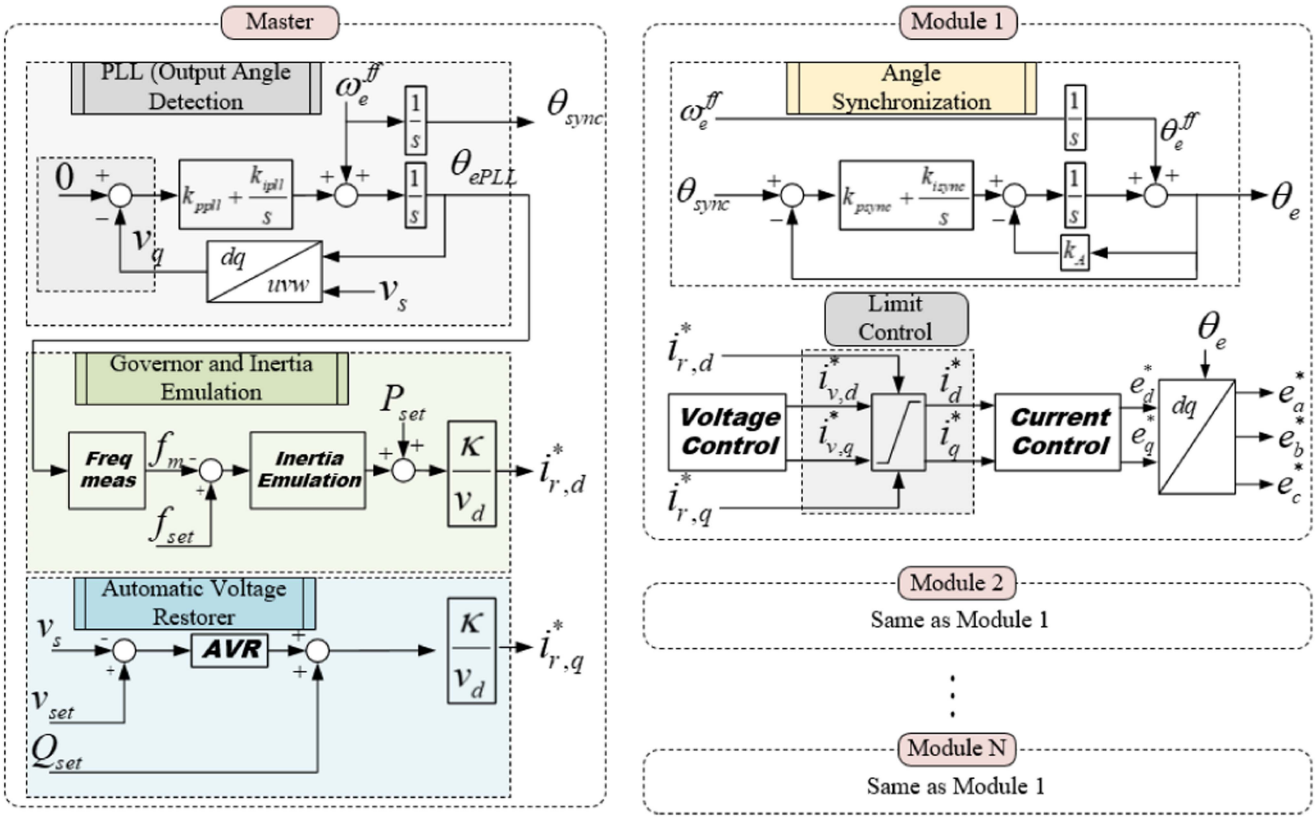

FIGURE 7. Proposed control concept for MPIS.

In practice, the PLL is used to control the behavior of power converters to emulate the inertia and synchronization characteristics of synchronous generators, by fine-tuning the PLL gains.

C. VECTOR CURRENT CONTROL

The speed governor and AVR control loops within the VSM generate supplementary current references for the virtual current source, enabling the adjustment of reactive power and mechanical input power to regulate voltage and frequency, respectively. This system operates through two primary functional control loops. 1) Frequency adjustment concerning active power: Changes in active power prompt adjustments in frequency. 2) Voltage adjustment concerning reactive power: Variations in reactive power result in voltage adjustments.

The droop expressions (23) and (24) encapsulate the above ideas

$$\frac{\Delta\omega}{\omega_{set)}} = k_{\omega}(s) \cdot \frac{\Delta P}{P_{\text{set}}} \tag{23}$$

$$\frac{\Delta v}{v_{\text{set}}} = k_{v}(s) \cdot \frac{\Delta Q}{Q_{\text{set}}}. \tag{24}$$

In addition, the speed governor in synchronous generators and the AVR play crucial roles. They function to generate the current references, $i^*_{r,d}$ and $i^*_{r,q}$, by continually adjusting and maintaining the power equilibrium during steady-state operation. Expressions (25) and (26) represent the current control loop

$$i^*_d = \frac{\kappa}{v_d} \cdot (P_{\text{set}} + G_M(f_{\text{set}} - f_m)) \tag{25}$$

$$i^*_q = \frac{\kappa}{v_d} \cdot (Q_{\text{set}} + G_{\text{avr}}(s)(v_{\text{set}} - v_s)). \tag{26}$$

IV. VALIDATION

A. EXPERIMENT SETUP

In this study, a 300 kW MPIS was employed for verification, utilizing three parallel modules. The experimental setup was meticulously designed to comprehensively evaluate the performance of the proposed control concept under various operational conditions.

On the ac side, all inverter modules were integrated with *LCL* filters to mitigate harmonic distortion and improve grid compatibility. These modules were connected to the grid via a delta-wye transformer, facilitating grid integration, and voltage transformation. Notably, the voltage sensor for each module was strategically positioned at the ac coupling point post-*LCL* filter, deviating from conventional capacitor voltage sensing methods. This strategic placement ensured accurate voltage measurement and enhanced control performance.

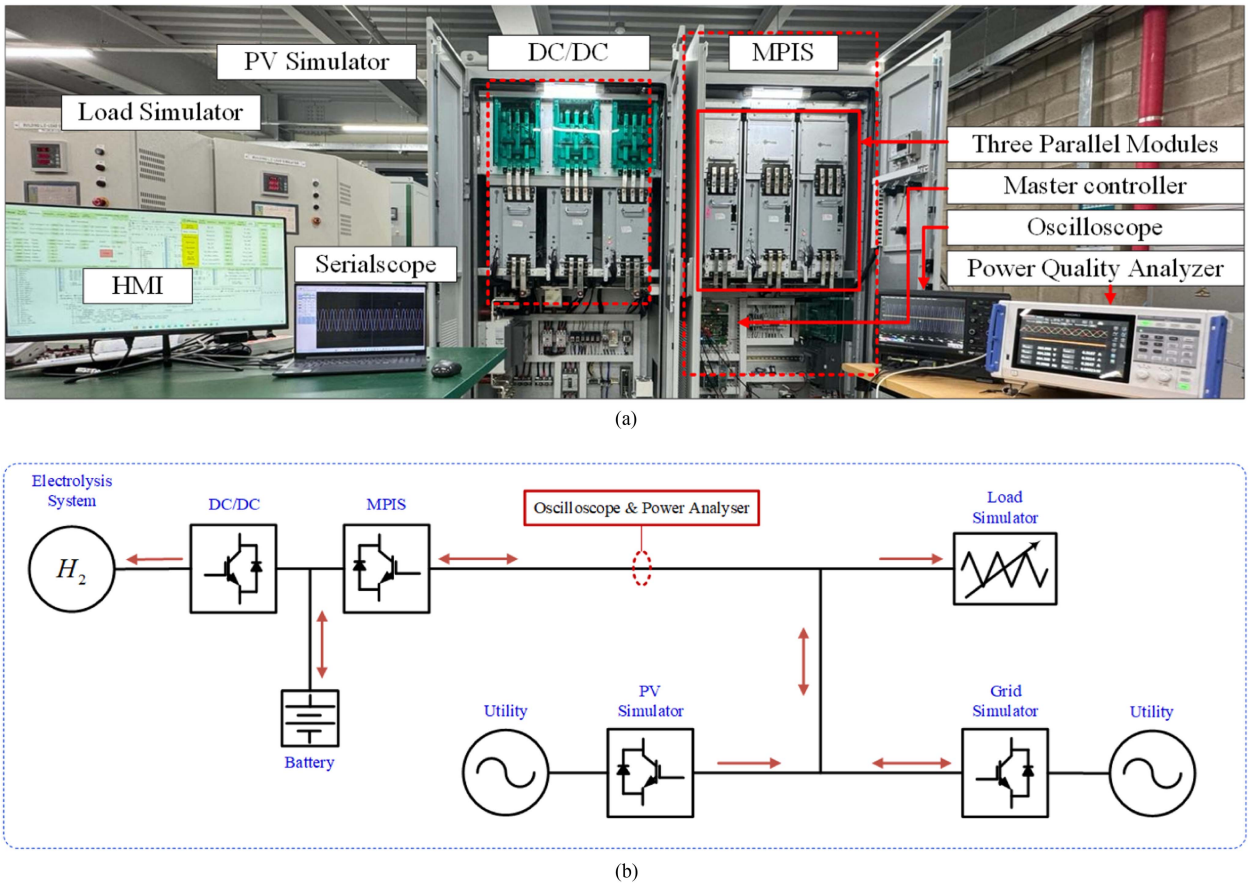

FIGURE 8. Typical MPIS for experimental validation. (a) Environment picture. (b) Single line diagram.

Similarly, on the dc side, all modules were interconnected to ensure synchronized operation and efficient power sharing. This interconnected configuration facilitated coordinated control and optimal utilization of resources within the MPIS.

To assess the efficacy of the proposed control concept in SA operation scenarios, a 300 kW dummy load was connected to the ac terminals of the MPIS. This dummy load setup enabled rigorous testing under varying load conditions, allowing us to gauge system stability and performance in isolation from the grid.

In addition to the dummy load setup, a photovoltaic (PV) simulator was incorporated to emulate the characteristics of RESs. This PV simulator was intricately coupled with the grid, as depicted in Fig. 8, replicating real-world scenarios and enhancing the experiment's realism. By simulating the behavior of RESs, we could evaluate the MPIS's response to fluctuations in renewable energy generation and assess its ability to maintain grid stability under dynamic conditions.

1) MPIS SPECIFICATIONS

The hardware parameters of the MPIS, and control parameters were meticulously documented and provided in Table 1. Each module of the MPIS is equipped with multi-parallel vector current control inverters, offering a rated power of 100 kW per module. The MPIS operates with a dc voltage of 700 V and converts it to an ac output voltage of 380 V at a frequency of 60 Hz, achieving an efficiency of

TABLE 1. Specifications for One (1) Module in MPIS

Symbol	Quantity	Value	Unit
P_N	Nominal Power	100	kW
V_N	Nominal Voltage	380	V
f_N	Nominal Frequency	60	H_z
L_{if}	Inverter Side Inductance	150	μH
L_{gf}	Grid Side Inductance	100	μH
C_f	Filter Capacitance	100	μF
f_{sw}	Switching Frequency	5	kH_z
k_G	Frequency Droop Control	32	pu
M	Inertia Coefficient	8	pu
$k_{p,pll}$	Proportional Gain (PLL)	5e-4	pu
$k_{i,pll}$	Integral Gain (PLL)	0.11	pu
$k_{p,sync}$	Proportional Gain (SYNC)	10	pu
$k_{i,sync}$	Integral Gain (SYNC)	10	pu

97%. The control strategy employed is a variant of the VSM control, which provides several protective features, including overvoltage, undervoltage, overcurrent, and overtemperature protections. This comprehensive dataset facilitated accurate replication and analysis, ensuring robustness and reliability in the experimental results. We could reference this documentation to validate experimental setups, verify simulation models, and compare results across different studies, fostering transparency and reproducibility in research findings.

2) OPERATION MODES

The MPIS operates in three primary modes to adapt to various grid conditions and operational needs. In grid-connected mode, the MPIS synchronizes with the grid, offering voltage support, frequency support, and inertia while facilitating seamless power transfer between P2G and the main grid. In SA Mode, the MPIS operates independently from the grid, supplying power directly to local loads. This mode is particularly crucial during black-start operations and grid failures. The transition mode allows the MPIS to switch between grid-connected and SA operations, ensuring an uninterrupted power supply and maintaining stability during grid disturbances.

3) ACTUAL FUNCTIONS

The MPIS performs several key functions to enhance grid stability and efficiency. The main feature is to harvest the excess power from renewable sources and send it to electrolysis system. It ensures synchronization, aligning voltage, frequency, and phase with the grid. The system provides inertia by emulating the behavior of synchronous generators, which is essential for grid stability. Voltage and frequency are maintained within prescribed limits, assisting in stabilizing grid voltage and frequency during fluctuations. The MPIS also features a current compensation mechanism to prevent cross-circulating currents between parallel modules, ensuring stable and efficient operation. In addition, it manages dynamic load conditions by adjusting power output to maintain balance among modules, adapting to changing load demands. Table 2 includes the MPIS input and output data that it processes to ensure a clear understanding of its role in enhancing grid stability through efficient P2G operations.

B. EXPERIMENTAL RESULTS

In this section, we dive into the empirical results of the implementation of the proposed MP-VCC concept on the MPIS in a P2G system.

1) ANGLE SYNCHRONIZATION OF MODULES

Fig. 9(a) shows the phase angles exhibited by the parallel modules prior to the synchronization process. The experimental results reveal significant differences in the phase angles among the modules, indicating a lack of coordination and synchronization. These disparities can lead to inefficient power transfer, increased losses, and potential stability issues within the power system.

Following the synchronization process, Fig. 9(b) illustrates the harmonization of phase angles among parallel modules. Experimental data demonstrate a notable reduction in phase

TABLE 2. MPIS Input and Output Data

Parameter	Input Data	Output Data
Excess Power	Renewable Source Power Input: Variable	DC Power Output: Variable
DC Power	Battery Power Input: Variable	AC Power Output: Variable
Control Signals	VSM Control Signals, Synchronization Commands	Inverter Status, Voltage and Current Feedback
Environmental Data	Temperature, Humidity, Grid Status	Operational Status, Fault Alarms
Performance Metrics	Inertia Requirements, Voltage and frequency Levels	Inertia Provision, Voltage and support Support Metrics

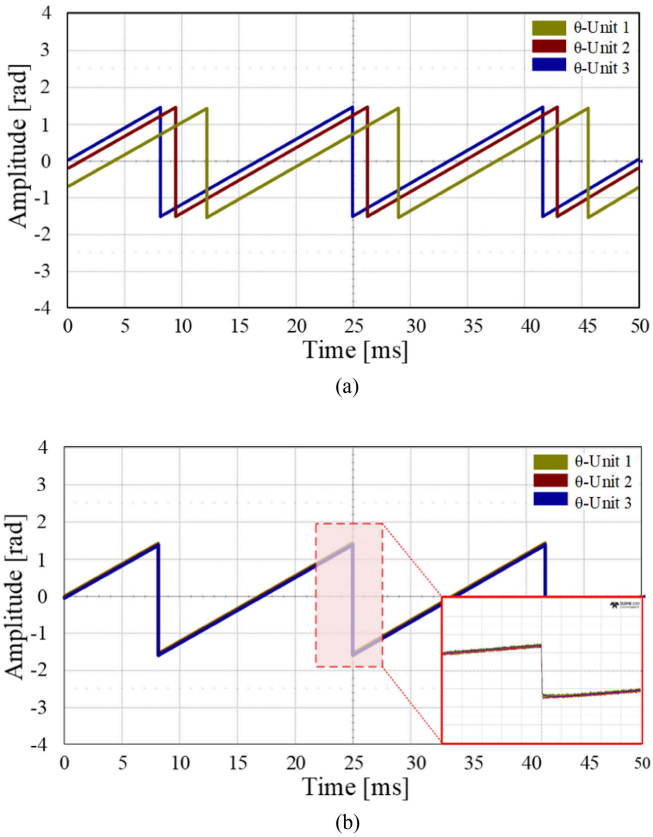

FIGURE 9. Phase angle of units in MPIS (a) before synchronization and (b) after synchronization.

angle disparities, indicating successful synchronization orchestrated by the synchronization signal transmitted through the eCAN communication bus. Harmonized phase angles enable efficient power sharing and enhance system stability, improving overall performance and reliability.

The high-speed eCAN communication bus plays a crucial role in transmitting synchronization signals from the central controller to the local controllers. Experimental results highlight the effectiveness of the communication bus in facilitating rapid and accurate synchronization, despite potential challenges such as signal delays and noise. The reliability and efficiency of the communication bus contribute significantly to the successful coordination of parallel modules, enhancing the resilience of power systems.

2) BLACK START SCENARIO

During black start operations without angle synchronization of modules, the MPIS experiences high starting and cross-circulating currents, leading to challenges in initiating system operation. Experimental data, as illustrated in Fig. 10, indicate erratic behavior in the output power of each module, output voltage, and phase currents, respectively. They reflect the difficulty in achieving stable operation without the angle synchronization of modules. These findings underscore the limitations of the MPI system in autonomously initiating grid restoration under black start conditions without proper synchronization mechanisms.

Following the angle synchronization of modules, the MPI system successfully initiates SA operation, as evidenced by the experimental results. Fig. 10(a) demonstrates consistent output power from each module, indicating synchronized operation and effective coordination between system components. Similarly, Fig. 10(b) illustrates stable load voltage, and Fig. 10(c) shows well-balanced phase currents for each module during SA operation with a 300 kW load connected to the ac terminals. These results highlight the critical role of angle synchronization of modules in overcoming the challenges posed by high starting and cross-circulating currents during black start scenarios, ensuring reliable system operation and grid restoration.

3) TRANSIENT SCENARIO

The test results depicted in Figs. 11 and 12 compare the power and current characteristics of the MPIS before and after implementing the current compensation concept. In Test Scenario 1, a full load step test was conducted utilizing the proposed MP-VCC concept without current compensation. At t = 0.05 s (see Fig. 11), the load transitioned from 0 to 300 kW. However, the output power for each module exhibited instability, indicating an inability to balance currents without compensation. Notably, even before the load step, cross-circulating currents were observed at no-load conditions. In Test Scenario 2, the same full load step test was repeated, but this time incorporating the current compensation method. At t = 0.05 s (see Fig. 12), the load transitioned from 0 to 300 kW. In contrast to the previous scenario, the output powers of all modules were balanced, and cross-circulating currents among parallel modules were effectively eliminated.

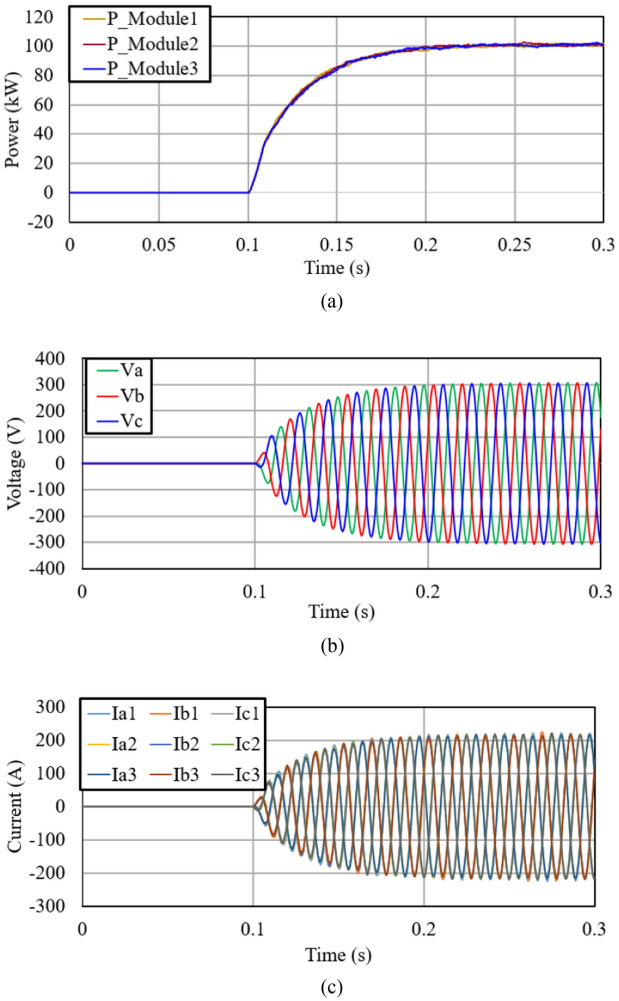

FIGURE 10. Black start operation (a) MPIS output power for each module, (b) MPIS output voltage, and (c) MPIS output phase currents for each module.

4) GRID SYNCHRONNIZATION SCENARIO

The amplitude of the inverter output voltage is usually controlled to match the grid voltage amplitude during synchronization. This ensures a smooth transition when connecting the inverter to the grid. The frequency of the inverter output voltage gradually adjusts to match the grid frequency. This process is essential for achieving synchronization between the inverter and the grid. The inverter adjusts its output voltage (blue), frequency and phase to synchronize with the grid voltage (green) as can be seen in Fig. 13. This synchronization process ensures that the inverter operates in harmony with the grid. The load current waveform represents the current flowing from the inverter into loads during synchronization. Proper synchronization ensures that the load current

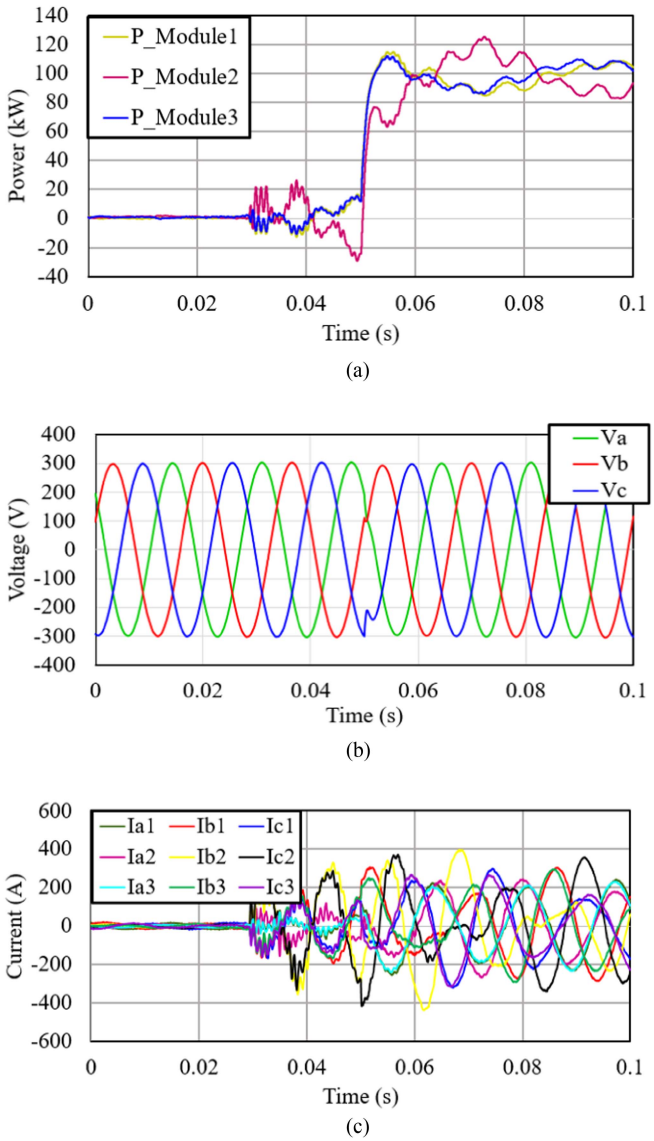

FIGURE 11. Load step test scenario before adding a current compensation loop (a) MPIS output power for each module, (b) MPIS out voltage, and (c) MPIS output phase currents for each module.

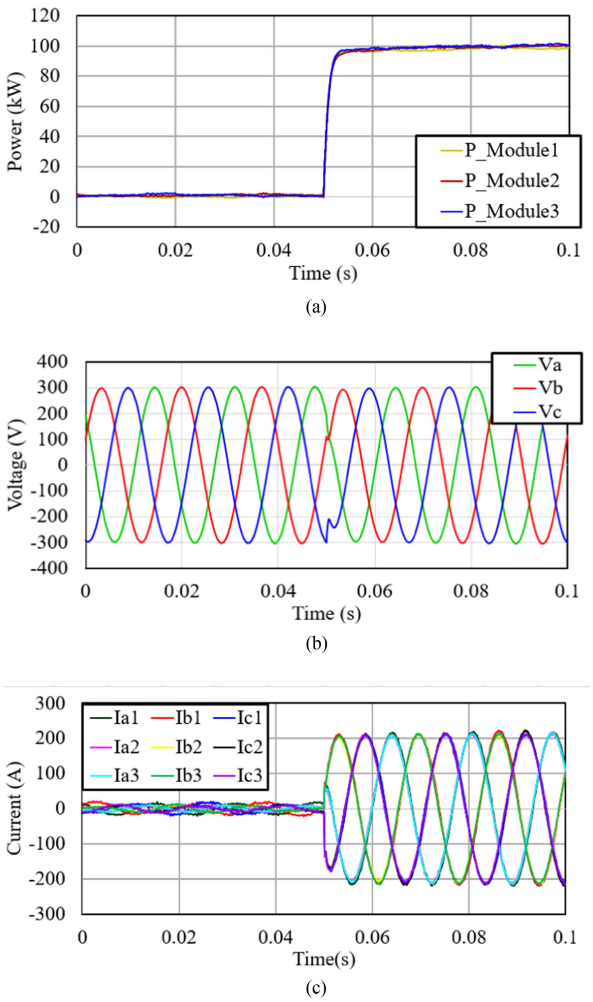

FIGURE 12. Load step test scenario after adding a current compensation loop (a) MPIS output power for each module, (b) MPIS out voltage, and (c) MPIS output phase currents for each module.

is in phase with the grid voltage, minimizing reactive power exchange and maximizing power transfer efficiency. During the synchronization period, the inverter continuously adjusts its output voltage frequency and phase based on feedback from the grid voltage, and the synchronization signal triggers when the process completes. This iterative process ensures precise alignment between the inverter and the grid, enabling seamless integration of MPIS and maintaining grid stability.

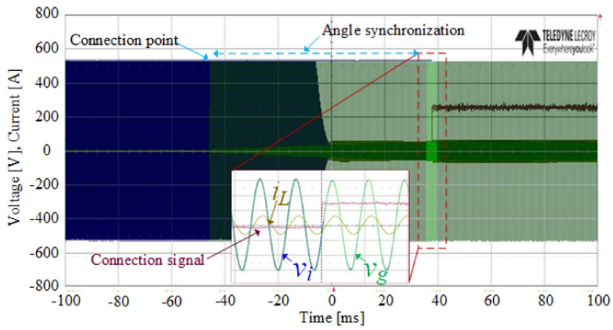

FIGURE 13. Grid synchronization and bumpless mode transition from SA mode to grid connection mode.

5) UNPLANED BLACK-OUT SCENARIO

The scenario depicted in Fig. 14 illustrates a critical black-out situation within the power grid. This occurrence occurs abruptly during normal operation when the grid voltage is unexpectedly severed. Despite this disruption, the loads connected to the ac terminal continue to receive power, albeit intermittently, thanks to the MPIS and the proposed MP-VCC concept. The graph portrays this transition with clarity: both

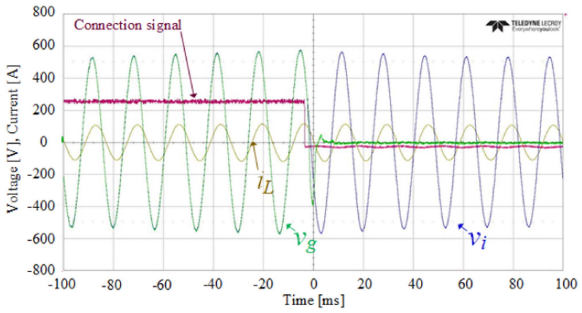

FIGURE 14. Unplanned black-out operation and bumpless mode transition from grid connection mode to SA.

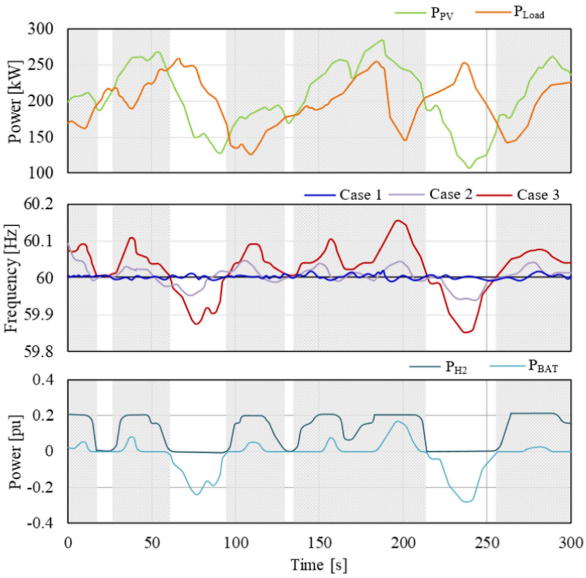

FIGURE 15. Inertial response. (a) PV output power versus load power for 5 min. (b) Line frequency for three test scenarios, and electrolysis power (P_{H2}) and battery power (P_{BAT}).

the inverter output voltage (depicted in blue) and the grid voltage (in green) overlap until the blackout, indicated by the disconnection signal (in pink). The load current (in yellow) maintains a consistent level both before and after the blackout, emphasizing the system's resilience despite the sudden loss of grid connectivity. This scenario underscores the importance of robust backup systems, such as MPIS in ensuring uninterrupted power supply during unforeseen grid disturbances.

6) INERTIAL RESPONSE AND GRID SUPPORT

Impact of Renewable Energy Integration:

Experimental studies in Fig. 15 have shown that the fluctuation of RES, such as wind and solar energy, can significantly reduce system inertia due to their inherent intermittency. However, innovative control strategies, such as the proposed virtual inertia and synthetic inertia emulation provided by MPIS, have demonstrated promising results in compensating for the loss of natural inertia by supporting the power system. These experiments emphasize the importance of developing grid support mechanisms tailored to the characteristics of renewable energy resources.

Effectiveness of energy storage systems (battery and hydrogen storage systems):

Energy storage systems have been subjected to extensive experimental testing to evaluate their effectiveness in providing rapid response during grid disturbances. Experimental results in Fig. 15 have highlighted the ability of ESS to augment inertial response by injecting or absorbing power instantaneously, thereby stabilizing frequency deviations. The battery and hydrogen storage systems have been used not only to challenge the issues related to the limited energy storage capacity and degradation over time but also to challenge the climate change issue by producing green hydrogen.

Role of advanced control strategies:

Advanced control algorithms, such as droop control, and current control have been investigated through experimental validation to confirm the contribution of the proposed control method and to enhance the coordination of MPIS. Experimental findings in Fig. 15 have demonstrated the efficacy of the proposed MP-VCC scheme implemented in improving the overall stability and resilience of power systems, particularly under dynamic operating conditions. Moreover, the integration of the current compensation technique for MPIS control modeling and synchronization control has shown promising results in optimizing grid support mechanisms based on real-time data.

Following the implementation of the proposed control concept, the test results in Fig. 15, Case 1 witnessed a remarkable reduction in line frequency fluctuation, with a staggering 93.4% decrease compared to the worst-case scenario (Case 3), where only PV generation was considered. This significant improvement underscores the effectiveness of the proposed method in stabilizing frequency fluctuations. In contrast, Case 2, employing droop-based current control, achieved a reduction of 54.7% in frequency deviation. While this reduction is notable, it pales in comparison to the remarkable efficacy demonstrated by the proposed control concept in Case 1. These findings underscore the superiority of the proposed method in mitigating frequency fluctuations and ensuring grid stability.

V. CONCLUSION

The novel control approach presented in this article, derived from VSM control and tailored for MPIS, offers a comprehensive solution to enhance grid stability in P2G conversion systems. Leveraging the inherent advantages of VSM control, including inertia provision, voltage support, and autonomous operation capabilities, the proposed methodology demonstrates remarkable performance in various grid conditions, including weak grids and SA operation scenarios. Through rigorous experimentation and validation, the efficacy of the proposed control strategy has been substantiated.

Experimental results illustrate the successful implementation of modules angle synchronization, enabling seamless

coordination among parallel units. Furthermore, during black-start operations, the MPIS system exhibits resilience, initiating SA mode without issues, even in the absence of grid synchronization. In addition, steady-state operation demonstrates the effectiveness of the implemented current compensation algorithm in mitigating cross-circulating currents, thus enhancing system stability and efficiency.

Transient tests confirm the capability of the proposed MP-VCC concept, with and without current compensation, to maintain balanced output powers among parallel modules, even during abrupt load transitions. Moreover, grid synchronization experiments highlight the MPIS's ability to seamlessly integrate with the grid, ensuring precise alignment of voltage, frequency, and phase for efficient power transfer.

In critical blackout scenarios, the MPIS demonstrates robustness, providing uninterrupted power supply to connected loads despite sudden grid disconnections. This resilience underscores the importance of backup systems, such as MPIS, in ensuring grid stability and reliability.

In general, the experimental findings validate the efficacy and robustness of the proposed control method, positioning it as a promising solution to improve grid stability while facilitating efficient P2G conversion operations. Future research avenues may explore the further optimization and scalability of the proposed approach for broader applications in renewable energy integration and improved grid stability.

REFERENCES

[1] J. Li, G. Li, S. Ma, Z. Liang, Y. Li, and W. Zeng, "Modeling and simulation of hydrogen energy storage system for power-to-gas and gas-to-power systems," *J. Modern Power Syst. Clean Energy*, vol. 11, no. 3, pp. 885–895, May 2023.

[2] Z. Cao, J. Wang, Q. Zhao, Y. Han, and Y. Li, "Decarbonization scheduling strategy optimization for electricity-gas system considering electric vehicles and refined operation model of power-to-gas," *IEEE Access*, vol. 9, pp. 5716–5733, 2021.

[3] X. Xing, J. Lin, Y. Song, Y. Zhou, S. Mu, and Q. Hu, "Modeling and operation of the power-to-gas system for renewables integration: A review," *CSEE J. Power Energy Syst.*, vol. 4, no. 2, pp. 168–178, Jun. 2018.

[4] Y. Jiang and L. Guo, "Research on wind power accommodation for an electricity-heat-gas integrated microgrid system with power-to-gas," *IEEE Access*, vol. 7, pp. 87118–87126, 2019.

[5] G. Rusatira, G. Park, and K. Lee, "Optimal grid supporting power-to-gas (GS-P2G) concept for grid voltage and frequency regulation," *IEEE Access*, vol. 11, pp. 42713–42724, 2023.

[6] B. Li et al., "Modeling integrated power and transportation systems: Impacts of power-to-gas on the deep decarbonization," *IEEE Trans. Ind. Appl.*, vol. 58, no. 2, pp. 2677–2693, Mar./Apr. 2022.

[7] H. Chen, P. Xuan, Y. Wang, K. Tan, and X. Jin, "Key technologies for integration of multitype RESs–Research on multi-timeframe robust scheduling/dispatch," *IEEE Trans. Smart Grid*, vol. 7, no. 1, pp. 471–480, Jan. 2016.

[8] T. Strasser et al., "A review of architectures and concepts for intelligence in future electric energy systems," *IEEE Trans. Ind. Electron.*, vol. 62, no. 4, pp. 2424–2438, Apr. 2015.

[9] M. Srikanth, Y. V. P. Kumar, M. Amir, S. Mishra, and A. Iqbal, "Improvement of transient performance in microgrids: Comprehensive review on approaches and methods for converter control and route of grid stability," *IEEE Open J. Ind. Electron. Soc.*, vol. 4, pp. 534–572, Oct. 2023.

[10] H. -J. Moon, Y. -J. Kim, and S. -I. Moon, "Frequency-based decentralized conservation voltage reduction incorporated into voltage-current droop control for an inverter-based islanded microgrid," *IEEE Access*, vol. 7, pp. 140542–140552, 2019.

[11] M. Vygoder, G. Oriti, J. Gudex, T. M. Tencate, A. L. Julian, and R. Cuzner, "Comparison of voltage abnormality detection methods for single-phase inverters to meet the requirements in IEEE Standard 1547-2018," *IEEE Trans. Ind. Appl.*, vol. 57, no. 5, pp. 4981–4990, Sep./Oct. 2021.

[12] W. Wang, Y. Li, Y. Cao, U. Häger, and C. Rehtanz, "Adaptive droop control of VSC-MTDC system for frequency support and power sharing," *IEEE Trans. Power Syst.*, vol. 33, no. 2, pp. 1264–1274, Mar. 2018.

[13] X. Meng, J. Liu, and Z. Liu, "A generalized droop control for grid-supporting inverter based on comparison between traditional droop control and virtual synchronous generator control," *IEEE Trans. Power Electron.*, vol. 34, no. 6, pp. 5416–5438, Jun. 2019.

[14] W. Wu et al., "Sequence-impedance-based stability comparison between VSGs and traditional grid-connected inverters," *IEEE Trans. Power Electron.*, vol. 34, no. 1, pp. 46–52, Jan. 2019.

[15] H. Nian and L. Li, "Direct power control of doubly fed induction generator without phase-locked loop under harmonically distorted voltage conditions," *IEEE Trans. Power Electron.*, vol. 33, no. 7, pp. 5836–5846, Jul. 2018.

[16] L. Huang et al., "A virtual synchronous control for voltage-source converters utilizing dynamics of DC-link capacitor to realize self-synchronization," *IEEE Trans. Emerg. Sel. Topics Power Electron.*, vol. 5, no. 4, pp. 1565–1577, Dec. 2017.

[17] Q. -C. Zhong, P. -L. Nguyen, Z. Ma, and W. Sheng, "Self-synchronized synchronverters: Inverters without a dedicated synchronization unit," *IEEE Trans. Power Electron.*, vol. 29, no. 2, pp. 617–630, Feb. 2014.

[18] V. Gurugubelli, A. Ghosh, and A. K. Panda, "Parallel inverter control using different conventional control methods and an improved virtual oscillator control method in a standalone microgrid," *Protection Control Modern Power Syst.*, vol. 7, no. 3, pp. 1–13, Jul. 2022.

[19] A. Quedan, W. Wang, D. Ramasubramanian, E. Farantatos, and S. Asgarpoor, "An adaptive virtual oscillator control structure for grid-forming inverters," *IEEE Syst. J.*, vol. 17, no. 3, pp. 3447–3455, Sep. 2023.

[20] M. A. Awal and I. Husain, "Unified virtual oscillator control for grid-forming and grid-following converters," *IEEE Trans. Emerg. Sel. Topics Power Electron.*, vol. 9, no. 4, pp. 4573–4586, Aug. 2021.

[21] L. Kong, Y. Xue, L. Qiao, and F. Wang, "Enhanced synchronization stability of grid-forming inverters with passivity-based virtual oscillator control," *IEEE Trans. Power Electron.*, vol. 37, no. 12, pp. 14141–14156, Dec. 2022.

[22] Z. Shao, X. Zhang, F. Wang, and R. Cao, "Modeling and elimination of zero-sequence circulating currents in parallel three-level T-type grid-connected inverters," *IEEE Trans. Power Electron.*, vol. 30, no. 2, pp. 1050–1063, Feb. 2015.

[23] R. Zhu, M. Liserre, Z. Chen, and X. Wu, "Zero-sequence voltage modulation strategy for multiparallel converters circulating current suppression," *IEEE Trans. Ind. Electron.*, vol. 64, no. 3, pp. 1841–1852, Mar. 2017.

[24] Z. Liang, X. Lin, X. Qiao, Y. Kang, and B. Gao, "A coordinated strategy providing zero-sequence circulating current suppression and neutral-point potential balancing in two parallel three-level converters," *IEEE Trans. Emerg. Sel. Topics Power Electron.*, vol. 6, no. 1, pp. 363–376, Mar. 2018.

[25] P. Albrechtowicz and P. Cisek, "An impact of the line resistance on the power flow calculations with installed phase-shifting transformer in different voltage levels power systems," *Electric Power Syst. Res.*, vol. 209, Aug. 2022, Art. no. 107970.

[26] N. Yaabari, P. Otubu Odu, and O. O. Ojah, "Impact of high voltage transmission on I^2r losses using a simplified ETAP model," *Amer. J. Eng. Res.*, vol. 10, no. 12, pp. 208–213, 2021.

[27] A. Narula, P. Imgart, M. Bongiorno, M. Beza, J. R. Svensson, and J. -P. Hasler, "Voltage-based current limitation strategy to preserve grid-forming properties under severe grid disturbances," *IEEE Open J. Power Electron.*, vol. 4, pp. 176–188, Feb. 2023.

[28] M. Schweizer, S. Almér, S. Pettersson, A. Merkert, V. Bergemann, and L. Harnefors, "Grid-forming vector current control," *IEEE Trans. Power Electron.*, vol. 37, no. 11, pp. 13091–13106, Nov. 2022.

[29] A. Belila et al., "Virtual synchronous generators for voltage synchronization of a hybrid PV-diesel power system," *Int. J. Elect. Power Energy Syst.*, vol. 117, 2020, Art. no. 105677.

[30] G. Rusatira, G. Park, and K. Lee, "PLL-based inertia emulation for grid supporting power-to-gas systems," in *Proc. 2023 IEEE Energy Convers. Congr. Expo. (ECCE)*, Nashville, TN, USA, Oct. 2023, pp. 927–933.

GEDEON RUSATIRA received the B.S. degree in electrical engineering from Rwanda National University, Huye, Rwanda, in 2013, and the M.S degree in electrical engineering from Chungbuk National University, Cheongju, South Korea, in 2016. He is currently working toward the Ph.D. degree in electrical engineering with the Tech University of Korea, Siheung, South Korea.

Since 2016, he has been a Research Engineer with G-Philos.co., Ltd, Yongin, South Korea. His current research interests include power electronics, power quality problems and solutions, energy storage systems, renewable energy, grid support capabilities in grid following inverters, grid forming capabilities with inertia emulation, and global decarbonization through power-to-gas systems.

GAWOO PARK received the B.S. degree in electronics engineering from Hanbat National University, Daejeon, South Korea, in 1992, and the M.S degree in electrical engineering from Chungbuk National University, Cheongju, South Korea, in 1995.

From 1994 to 2004, he worked as a Research Engineer with POSCO ICT, Pohang, South Korea. From 2004 to 2009, he was the Director of the Research and Development Department with PLASPO, Goyang, South Korea. Since 2009, he has been the Chief Executive Officer and the Founder of G-Philos.co., Ltd, Yongin, South Korea. His current research interests include power electronic systems, renewable energy, energy management systems, energy storage systems, fuel cell systems, and global decarbonization through power-to-gas systems.

KYUNGSOO LEE (Member, IEEE) received the Ph.D. degree in electronics and information engineering from the Tokyo University of Agriculture and Technology, Tokyo, Japan, in 2008.

From 2008 to 2012, he was with the TOSHIBA Co., working on grid-connected photovoltaic inverter research and development. From 2012 to 2014, he was with Korea Institute of Energy Technology Evaluation and Planning. In 2014, he joined the Department of Energy and Electrical Engineering, Tech University of Korea, Siheung, South Korea, where he is an Associate Professor. He is currently working on the design of grid-connected distributed energy resources and photovoltaic system engineering.